JOURNAL OF MATERIALS SCIENCE: MATERIALS IN MEDICINE 12 (2001) 743–751

The spatial arrangement of tubules in human dentin

J. H. KINNEY[1]*, J. OLIVEIRA[2], D. L. HAUPT[3], G. W. MARSHALL[1], S. J. MARSHALL[1]
[1]*Division of Bioengineering and Biomaterials, Department of Preventive and Restorative Dental Sciences, University of California, San Francisco, San Francisco, CA 94143-0758*
[2]*Battelle Pacific Northwest Lab, Richland WA 99352*
[3]*Lawrence Livermore National Laboratory, Livermore, CA 94551*
E-mail: jkinney@itsa.ucsf.edu

We applied two-dimensional numerical methods to describe the spatial arrangement of tubules in human dentin. The methods considered were two-point correlation functions, entropy-like measures, and angular distributions between nearest neighbors. The correlation functions were based on Fourier transform methods. The latter two approaches were based on stochastic geometry, and involved developing the Delaunay tessellations of the tubule patterns and their dual Voronoi diagrams. We discovered that for analyzing the distribution of tubules the geometric methods of lattice tessellations were more sensitive to structural order of the tubules than were Fourier-based schemes. Analysis of the data indicated that dentinal tubules are highly ordered in normal dentin.

1. Introduction

Dentin is the hard, mineralized tissue in teeth that lies between the exterior enamel layer and the pulp. The most striking morphological feature of dentin is the tubule, which is a continuous cylindrical channel approximately 1–2 μm in diameter that runs between the dentin-enamel junction and the pulp. Tubules are surrounded by highly mineralized cuffs of peritubular dentin, and are imbedded in a matrix of mineralized collagen called intertubular dentin. Previous studies have described the distribution of tubules in human dentin in terms of the number density of tubules, tubule radius, and width of the peritubular cuff [1, 2]. This information has been used to interpret positional differences in the physical properties of dentin such as hardness and elastic modulus [3, 4].

In addition to the role that tubule density, orientation, and distribution might have in affecting mechanical behavior, tubule organization appears to play a significant role in demineralization and etching. In a previous study, we were able to explain the results of a controled demineralization experiment in terms of the tubule density and orientation with respect to the etching direction [5]. We hypothesized that the etching rate and resulting surface morphology were controled by the density and orientation of the tubules, which depend upon location within the dentin.

There are other reasons for a quantitative measure of tubule organization. Because the tubule lumens are the remnant homes of the odontoblast processes, knowledge of their organization might be helpful in understanding dentinogenesis or disease processes. A characteristic trait in dentinogenesis imperfecta, a heritable disorder of dentin, is few and irregular tubules in a disorganized collagen matrix. These histological observations have not been quantitative, largely because of the lack of a framework to describe tubule organization.

In cross section, the tubules look like an ensemble of circular holes. There are four generic ways that the tubules might be distributed on the cross section: (a) ordered on a periodic lattice; (b) disordered about periodic lattice sites; (c) clustered; or (d) randomly positioned within the intertubular matrix. Number density and size alone do not distinguish among these spatial distributions, so previous work is of limited value for understanding the spatial organization of the tubules.

In this study, we explored several two-dimensional numerical methods of describing point pattern distributions, and applied these methods to evaluate the tubule distributions near the dentin-enamel junction (primary outer dentin). The methods considered were two-point correlation functions, entropy-like measures, and angular distributions between nearest neighbors. The correlation functions were based on Fourier transform methods. The latter two approaches were geometric, and involved developing the Delaunay tessellations of the tubule patterns and their dual Voronoi diagrams. Though the principal focus was on the spatial arrangement of dentin tubules, the point pattern techniques described in this study are applicable to any materials problem where spatial arrangement of microstructure is important.

*Author to whom correspondence should be addressed: Department of Preventive and Restorative Dental Sciences, University of California, San Francisco, 707 Parnassus Ave, MS 0758, San Francisco, CA 94143-0758.

2. Materials and methods

Three freshly extracted third molars from females aged 19–23 were used in this study. The teeth were sterilized with gamma irradiation prior to use [6]. Each tooth was mounted in polymethylmethacrylate and radiographed to determine the location of the dentin-enamel junction with respect to the occlusal surface. Then each tooth was sectioned parallel to the occlusal surface and just below the dentin-enamel junction using a modified water-cooled low speed diamond saw (Isomet, Buehler Ltd., Lake Bluff, IL). The location of the specimens and the approximate orientation of the tubules are shown in Fig. 1. The cut disks were 0.75 mm thick. They were abraded flat on silicon carbide paper (grits 400, 600, and 800), and then polished using successive aluminum oxide slurries of 1.0-, 0.3-, and 0.05-μm particle size. Between polishing steps, each specimen was ultrasonicated to remove debris.

Each dentin disk was sectioned into four parts, and fiduciary marks were cut near the periphery close to the dentin-enamel junction. Each section was studied with a wet scanning electron microscope (modified ISI SX-40A SEM), which permitted imaging without prior desiccation or coating [7]. The instrument operated under a low pressure of approximately 10–100 m Torr, which suppressed charging but led to eventual desiccation of the sample. However, for mineralized dentin, no significant morphological changes have been detected during drying [8]. Selected areas of the four quadrants nearest the dentin-enamel junction were imaged and photographed at 20 kV and magnification of 2000 ×. The SEM images were digitized into 256-level gray scale images containing 512 × 384 picture elements (pixels). Magnification errors were minimized by checking microscope calibration against known standards, by viewing samples in an untilted configuration at the same working distance, and by determining the errors in magnification at different working distances.

2.1. Image processing

The SEM images were converted from gray scale to binary format with the pixels contained within the tubule lumens defined as occupied (pixel value of 1) and the dentinal hard tissue defined as unoccupied (pixel value of 0). These binary images were then segmented with a cluster-labeling algorithm so that each tubule was uniquely labeled (e.g. 1, 2, 3, . . . ,*N*). The number density of tubules, defined as the number of tubules per unit area, was calculated after labeling.

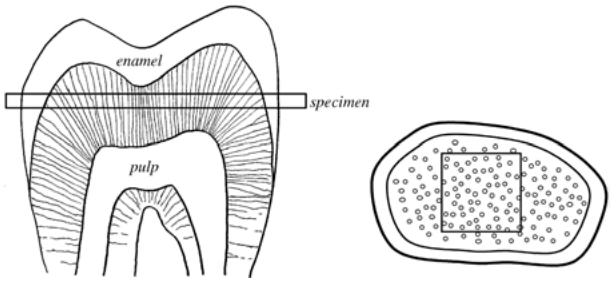

Figure 1 An artist's rendering showing the location of the cut specimen with respect to the coronal dentin. The lines crossing the dentin from the dentin-enamel junction to the pulp represent the tubule lumens. Though the tubule patterns are more complex than shown, in the center part of the occlusal section (shown on the right) the tubules intersect the cut surface at approximately right angles.

The two-point correlation functions were calculated for each of the binary images. Next, the center of gravity of each tubule lumen was calculated and used to define a point lattice for the tubule distribution. These lattice points were used as vertices of a Delaunay tessellation from which a Voronoi diagram was generated. The tessellations were subsequently analyzed according to methods described below. This analysis procedure, as followed for a typical SEM image of dentinal tubules, is shown in Fig. 2.

2.2. Test patterns

Four generic, discreet point patterns were created to explore the range of tubule distributions that might be observed in dentin. These patterns were created on a rectangular image space containing 512 × 384 pixels (corresponding to the digital image of the SEM). The generic patterns were: (1) a square (periodic) lattice of $m \times n$ points 50 pixels apart ($D_o = 50$); (2) a disordered lattice obtained by randomly displacing the tubules in a circular region about the periodic lattice sites of the $m \times n$ square grid; (3) a random lattice that approximated the complete spatial randomness of a Poisson point process; (4) groupings of points clustered about randomly positioned sites. Examples of these generic patterns are provided in Fig. 3.

Multiple images of the disordered, clustered, and random point patterns were created by varying the starting seed value of the random number generator. The disordered patterns were created by randomly distributing points in a circular region centered about the square lattice sites in terms of a maximum radius, D/D_o. The maximum radius ranged from 0.1 to 1.0 in equal increments. For each value of D/D_o, four point patterns were created starting with different seed values of the uniform random number generator. The root mean square tubule displacements differed slightly for each seed value, thereby allowing us to obtain a statistical measure of the accuracy of the methods used to describe the point pattern distributions.

Ten random point patterns were created with a uniform random number generator, the probability level for site occupancy set to approximate the range in tubule density seen with the SEM images (60–100 tubules per image). The same random number generator was also used to generate the lattices for the clustered patterns. For the clustered patterns, the probability level for site occupancy was set to provide anywhere from six to ten randomly distributed lattice sites per image. Ten points were then randomly distributed about each site in the same manner as used to construct the disordered point patterns, with the maximum displacement radius $D = 0.5\,D_o$.

2.3. Data analysis

The first two spatial correlation functions, S_n, are defined as

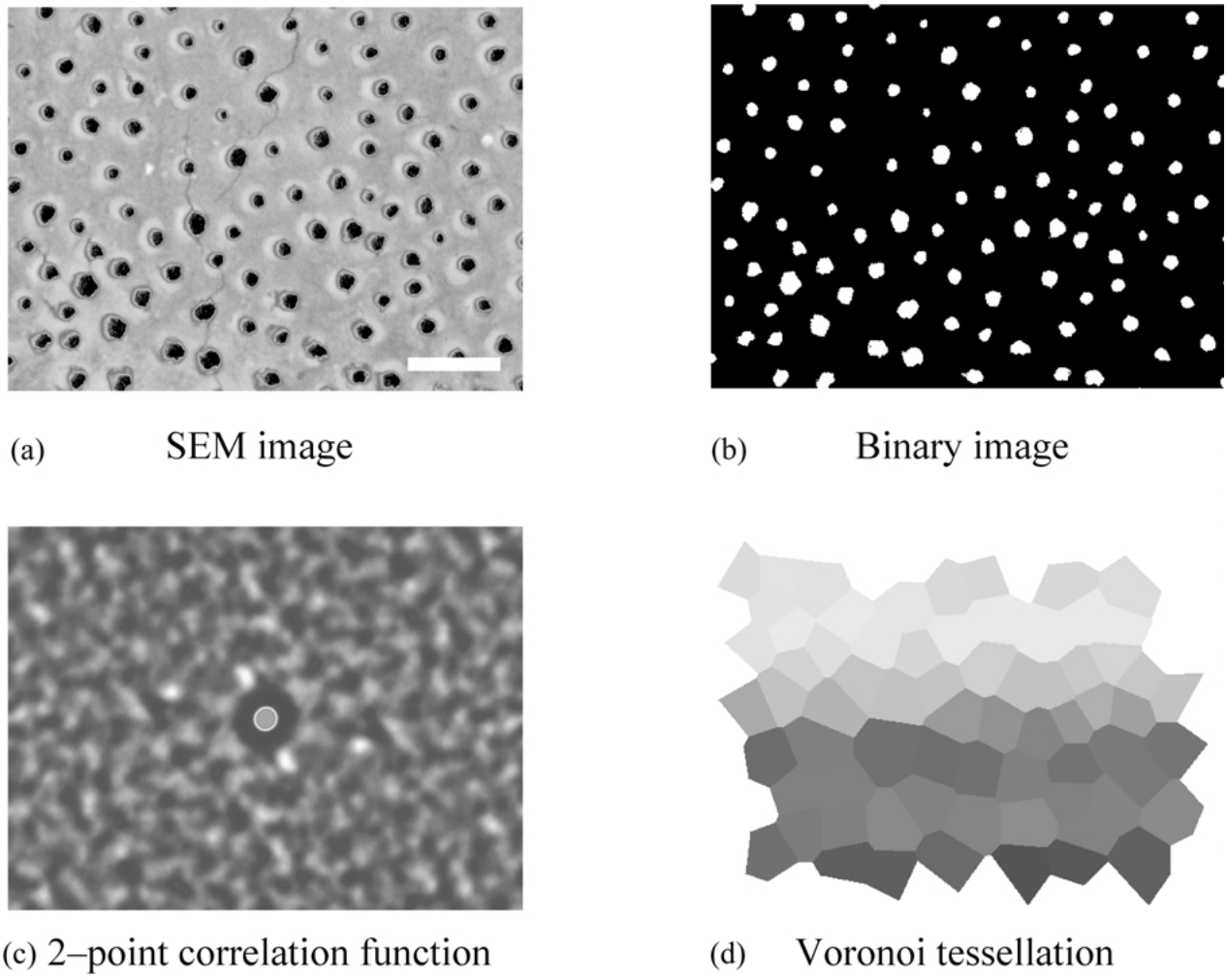

Figure 2 Representative stages in the image processing procedure used to analyze the distribution of tubules in human dentin: (a) the unprocessed SEM image of the tubules, (b) the resulting binary image, (c) the two-point correlation function S_2 of the binary image, and (d) the resulting Voronoi diagram. The bar in the SEM image represents 10 μm.

$$S_1 = \langle f(r) \rangle \qquad S_2 = \langle f(r) f(r+x) \rangle \tag{1}$$

Here, the brackets refer to an integration of the spatial coordinates r, and $f(r)$ is a characteristic function that estimates the spatial distribution of any two phases. For this analysis, intertubular and peritubular dentin were given the material value of 0, and tubule lumens were defined with material value of 1. Hence, $f(r) = 1$ for pixels occupied by tubules, and $f(r) = 0$ elsewhere.

The two-point correlation function, S_2, was calculated from the binary images with the help of the convolution theorem. The convolution theorem states that for any two functions $f(x)$ and $g(x)$ that have Fourier transforms $F(k)$ and $G(k)$, then

$$\int_{\infty}^{\infty} g(x) f(x+r)\, \mathrm{d}x = \int_{-\infty}^{\infty} F(k) G^*(k) \mathrm{e}^{-ikx}\, \mathrm{d}k \tag{2}$$

Here, $G^*(k)$ is the complex conjugate of $G(k)$. For a two-dimensional binary image given by $f(x, y)$ with Fourier transform $F(k, w)$, the convolution theorem allows us to write the two-point correlation function as

$$S_2(x) = FFT^{-1} \| F(k, w) \|^2 \tag{3}$$

Here, FFT^{-1} is the inverse Fourier transform.

The tubule centers of gravity (the set $S = \{S_1, S_2, \ldots S_n\}$ of n distinct tubules) were used as the vertices of a Delaunay triangular tessellation of the images $\mathscr{D}(S)$. Delaunay tessellation makes use of the property that all circumcircles of a Delaunay triangle are empty; that is, they contain no other vertices. In practice, any three near neighbor points (tubules) are joined together as a triangle if no other points reside within the circumcircle formed by the three points. If another tubule center of gravity does lie within the circumcircle, then the three points of the triangle do not satisfy the empty circumcircle criterion and new points must be chosen. Delaunay triangles are formed in this manner until all of the image space is tessellated.

The interior angles of each of the Delaunay triangles were determined with the inner product relationship from vector algebra. The minimum and maximum angles of each triangle were stored in separate arrays for later comparison with the angle distributions expected for complete spatial randomness.

Voronoi polygons were formed from the intersection of perpendicular bisectors of the sides of the Delaunay triangles. As with the Delaunay triangles, the Voronoi polygons tessellate the image space. The Voronoi polygons were used to calculate the Thiel's redundancy measure, R^*, defined as [9]

$$R^* = H_{\max} - H \tag{4}$$

Here, H is an entropy statistic used to define the tubule organization. $H_{\max}$ and H were determined from the areas

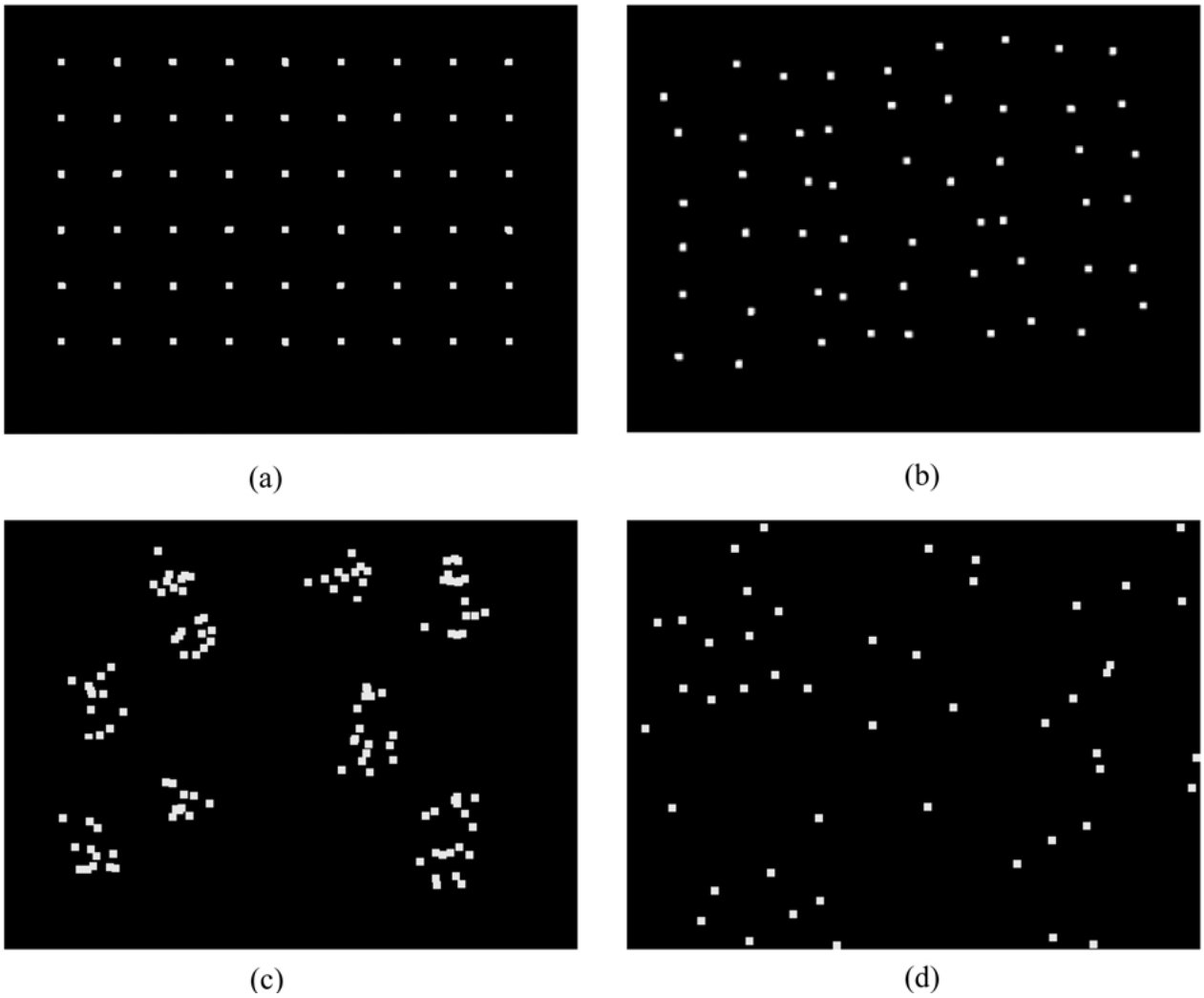

Figure 3 Simulated point patterns used for the analysis: (a) square array, (b) random displacements $(D = 0.15D_o)$ about the square lattice, (c) clustered point pattern, and (d) a random pattern created with a uniform random number generator.

of the Voronoi polygons following the method of Chapman [10]

$$H_{\max} = \ln(n)$$
$$p_i = \frac{A_i}{\sum_i A_i} \tag{5}$$
$$H = \sum_i p_i \ln(1/p_i)$$

Here, n was the number of tubules in the image, and A_i was the area of the ith Voronoi polygon. For these calculations, the contributions from the boundary polygons were excluded.

2.4. Statistical analysis

The distributions of both the minimum and maximum angles of $\mathscr{D}(S)$ were compared with a Chi-squared goodness of fit test between the observed frequencies and the expected frequencies of a theoretical distribution. Cells in the frequency distribution that contained fewer than five observations were combined with adjacent cells prior to the analysis. The expected frequencies used for comparison were obtained from the random lattice, the clustered lattice, and the square periodic lattice that had been displaced by 15%. A one-tailed probability of obtaining a value of χ^2 or greater (p) was also determined. The values of the redundancy measure, R^*, were compared using ANOVA.

3. Results

The two-point correlation function along the x-axis is shown in Fig. 4 for the square periodic lattice with lattice spacing D_o and two examples of the displaced lattices. The correlation functions, which were normalized to the volume fraction of simulated tubules in the images, have been truncated at a length scale of 1.5 D_o for clarity of discussion. The periodic grid (solid line) had a strong peak centered one lattice unit (D_o) away from the origin. The magnitude of this peak was approximately 80% of the main peak centered at the origin. The dashed line is the correlation function for a regular lattice that had been displaced by an average distance of 7%. The amplitude of the D_o peak was approximately one fourth that of the non-displaced lattice, and was not as well localized. The dotted line is representative of a lattice where the tubules had been displaced an average of 15%, and now the D_o peak was negligible and spread out over a considerable range.

The correlation function of a typical random distribution is compared with the correlation functions of two representative patterns of dentin tubules in Fig. 5. Unlike

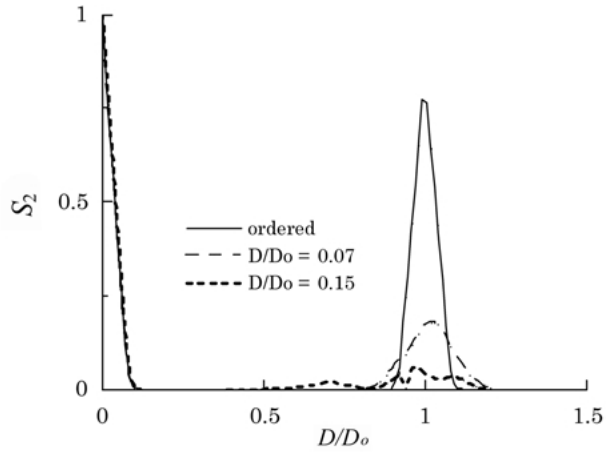

Figure 4 The two-point correlation function, S_2, as a function of radial distance D/D_o, where D_o is the lattice spacing for the periodic lattice. The solid line is the correlation function for the periodic square lattice; whereas, the dashed line and dotted line represent the correlation functions for $D/D_o = 0.07$ and $D/D_o = 0.15$, respectively. Slight displacements from perfect periodicity reduce and broaden the first neighbor peak at D_o.

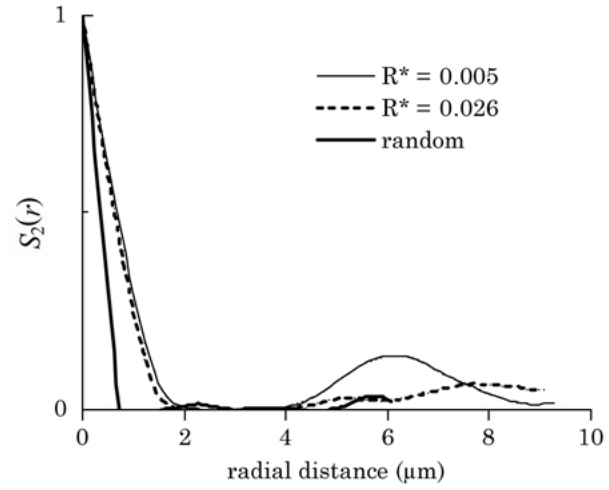

Figure 5 A comparison of S_2 calculated for two representative dentinal tubule patterns with the simulated random lattice. The tubule patterns represented the extremes of the observed order ($R^* = 0.005$) for the most ordered, and ($R^* = 0.026$) for the least ordered. S_2 had a broad peak centered near 6μm in the most ordered sample, but no short-range correlation in the less ordered sample. The width of the random pattern's central peak is less than that for the dentinal tubules because the simulated tubules were of smaller radius.

the periodic lattice, the random patterns did not show any significant peaks aside from the central peak at the origin. This central peak was narrower in the random pattern than for the SEM images of the tubules because the radii of the simulated tubules were smaller. S_2 of the tubule patterns also had an extended region of zero value, indicating that there was a well-defined minimum separation between the tubules. For the most highly ordered tubule pattern (corresponding to the smallest value of $R^* = 0.005$), there was a broad peak near 6 μm. No such peak was observed for the tubule pattern with the larger value of $R^*(= 0.026)$, which appeared much more like the random correlation pattern.

Results of some of the geometric measures of tubule organization are provided in Table I. These results are compared with the simulated patterns. The number density of tubules ranged from 20 to 40 thousand per square mm, consistent with those measured by others near the dentin-enamel junction. Values of R^* for the dentin specimens ranged from 0.016 to 0.024, whereas R^* averaged 0.128 and 0.467 for the random and clustered specimens, respectively. The variation of R^* with displacement from a periodic grid is shown in Fig. 6. R^* increased from zero (for no displacement) upwards of 0.08 for large average displacements. The expectation of R^* for a random Poisson point process (0.134) is shown as a solid line in this figure.

The distributions of minimum angles of the Delaunay triangles are provided in Table II for the simulated tubule patterns, the theoretical Poisson point process defining complete spatial randomness, and the dentin specimens. A similar listing of the distribution of maximum angles is given in Table III. The frequency distributions of the minimum angles for the simulated patterns are provided in Fig. 7, where we have used a bin size of 10°. The frequency distribution of the minimum angles of a typical dentin image is compared with those of the random distribution and a displaced lattice in Fig. 8. Results of the Chi-squared analyses for the maximum angles in $\mathscr{D}(S)$ are listed in Table V.

4. Discussion

In this study, we were interested in developing a stochastic geometric model of tubule organization within the dentin matrix. An initial analytic model that was chosen to describe this tubule organization was the random Poisson point process that approximates complete spatial randomness. Hence, we formed a null hypothesis that tubules were distributed randomly within the dentin matrix. Our task was one of finding a sensitive measure of organization that could differentiate between random and non-random tubule distributions.

Correlation functions are frequently used to describe texture, and have been used to provide better bounds for elastic [12] and transport [11] constants in heterogeneous materials. However, in this application S_2 was not

TABLE I Results of geometric properties of the tubule distributions in the dentin specimens and in the simulated lattices. N_A is the number density of the tubules (points), R^* is the Thiel's redundancy measure, and $\langle\alpha_m\rangle$ are the average minimum and maximum angles in $\mathscr{D}(S)$ respectively. Standard deviations are in parenthesis

Specimen	$N_A(\text{mm}^{-2}) \times 10^{-4}$	R^*	$\langle\alpha_{min}\rangle$ deg.	$\langle\alpha_{max}\rangle$ deg.
Dentin 1	2.76 (0.19)	0.016 (0.009)	38.5 (2.8)	91.5 (2.9)
Dentin 2	4.22 (0.83)	0.021 (0.011)	39.8 (1.0)	87.2 (1.2)
Dentin 3	2.53 (0.94)	0.024 (0.012)	39.2 (2.6)	88.7 (4.2)
Random	1.86–4.61	0.128 (0.026)	28.8 (14.0)	97.8 (25.4)
Clustered	2.30–3.26	0.467 (0.020)	23.7 (14.0)	106.1 (24.9)
Square periodic	2.59	0.000 (0.000)	45.0 (0.3)	89.6 (0.4)

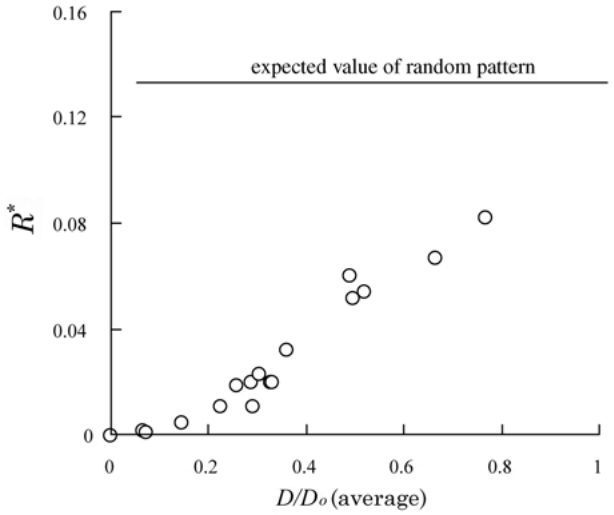

Figure 6 The value of Thiel's redundancy measure, R^*, as a function of the average random displacements about the square lattice sites. The expectation of R^* for complete spatial randomness is 0.134, a value never reached by random displacements about a periodic lattice.

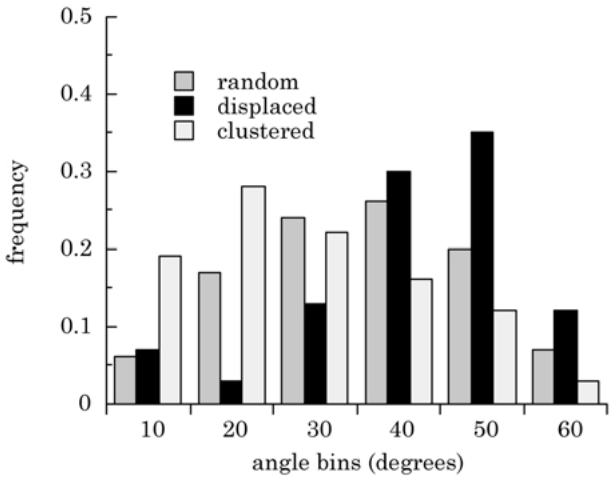

Figure 7 The frequency distribution of minimum angles of $\mathscr{D}(S)$ for random, displaced, and clustered lattices. The clustered lattice maintains a higher proportion of smaller angles because the Delaunay triangles at the cluster borders must span to distant points. The random lattice is symmetric about 30°, whereas the displaced lattice ($D/D_o = 0.20$) still contains a large number of high angle triangles.

sensitive in differentiating between order and disorder. Only in the few cases of greatest tubule order as determined by R^* did S_2 hint at any structural order. This was clearly observed in the behavior of S_2 with only slight displacements from the periodic lattice. An average, random displacement of only 0.07 D_o (7%) decreased the amplitude of the peak at D_o by a factor of four. By the time displacements had reached $0.15\,D_o$, there was no longer any evidence of structural order, although the square pattern was still apparent with visual inspection (Fig. 2b).

The sensitivity of S_2 to small changes in spatial order may be understood in terms of the properties of the Fourier transform. In a perfectly periodic system, all of the amplitude is carried by the few coefficients that define the characteristic frequencies of the pattern. Deviations from perfect periodicity require more terms in the Fourier expansion, thereby decreasing the amplitude of the fundamental peaks and delocalizing them as well. Because Fourier methods discard much of the geometric information, S_2 should not be expected to be a sensitive measure of small deviations from periodicity.

Other approaches to point pattern analysis consider the angular distribution between nearest neighbors. Boots [13] suggested selecting an angle at random from a

TABLE II Frequency distributions of the minimum angles in $\mathscr{D}(S)$ for the dentin specimens and the simulated lattices. The numbers are normalized to the average number of tubules (points) within the images

Specimen	0–10°	11–20°	21–30°	31–40°	41–50°	51–60°
Random (CSR)	0.06	0.17	0.24	0.26	0.20	0.07
Random pattern	0.06	0.17	0.23	0.28	0.19	0.07
Square periodic	0.00	0.00	0.00	0.00	1.00	0.00
Displaced 15%	0.00	0.00	0.01	0.26	0.64	0.09
Displaced 20%	0.07	0.03	0.13	0.30	0.35	0.12
Clustered	0.19	0.28	0.22	0.16	0.12	0.03
Dentin 1	0.05 (0.01)	0.06 (0.02)	0.10 (0.07)	0.33 (0.09)	0.35 (0.07)	0.11 (0.07)
Dentin 2	0.04 (0.02)	0.04 (0.02)	0.08 (0.01)	0.30 (0.06)	0.38 (0.02)	0.16 (0.06)
Dentin 3	0.07 (0.05)	0.04 (0.02)	0.08 (0.01)	0.27 (0.05)	0.43 (0.03)	0.11 (0.05)

TABLE III Frequency distributions of the maximum angles in $\mathscr{D}(S)$ for the dentin specimens and the simulated lattices. The numbers are normalized to the average number of tubules (points) within the images

Specimen	60–80°	81–100°	101–120°	121–140°	141–160°	161–180°
Random (CSR)	0.27	0.43	0.22	0.07	0.01	0.00
Random pattern	0.26	0.43	0.16	0.09	0.01	0.05
Square periodic	0.00	1.00	0.00	0.00	0.00	0.00
Displaced 15%	0.43	0.42	0.01	0.00	0.03	0.11
Displaced 20%	0.45	0.37	0.03	0.00	0.03	0.12
Clustered	0.17	0.35	0.24	0.13	0.08	0.03
Dentin 1	0.47	0.34	0.08	0.02	0.03	0.06
Dentin 2	0.54	0.28	0.06	0.04	0.05	0.03
Dentin 3	0.65	0.13	0.06	0.00	0.13	0.03
Dentin average	0.55	0.25	0.07	0.02	0.07	0.01

TABLE IV Results of Chi-square analysis of observed patterns with expected patterns for the minimum angles in $\mathscr{D}(S)$. The one-tailed probability of obtaining a value of χ^2 or greater is given by p

Observed frequency	Expected frequency	χ^2	p
Random lattice	Random (CSR)	0.12	0.99
Clustered	Random (CSR)	17.2	< 0.001
Displaced 15%	Random (CSR)	13.9	0.003
Dentin average	Random (CSR)	20.6	< 0.001
Dentin average	Clustered	69	0
Dentin average	Displaced 20%	0.93	0.92

random sampling of $\mathscr{D}(S)$. For this sampling procedure, it was possible to derive the probability distribution function, pdf, for a random Poisson point process [14].

Mardia *et al*. [15] noted that this method of sampling was inefficient, and proposed recording the minimum angles, α_{min}, from each Delaunay triangle. For sampling from a distribution of random points, they derived the following pdf for $\alpha_{min} (0 < \alpha_{min} < \pi/3)$:

$$f(\alpha_{min}) = \frac{2}{\pi}[(\pi - 3\alpha_{min})\sin(2\alpha_{min}) + \cos(2\alpha_{min}) - \cos(4\alpha_{min})] \quad (6)$$

The pdf for α_{min}, is shown in Fig. 9. For the random distribution, the pdf is a maximum at 30°. Integrating the pdf, we obtained the theoretical distribution of minimum angles for the ten degree bin sizes used in Table II.

Comparing the measured angle distributions of the simulated patterns, we can make some generalizations. The random distribution was peaked at 30°, and was only lightly populated near the tails of the angular range (0–10°; 51–60°), as expected from the pdf. The clustered patterns, on the other hand, had a significantly larger fraction of small angles due to the necessity of spanning to distant clusters. $\mathscr{D}(S)$ of the perfect square lattice formed 45° angles: α_{min} was identically 45° for each triangle. As the tubules became randomly displaced from the perfect square, α_{min} took on other values, although α_{min} remained clustered near 45° for the smallest displacements. The entire angular range, however, became populated by the time the average displacements had reached $D/D_o = 0.2$.

Chi-squared analysis was performed to test the hypothesis that the observed frequency was an accurate approximation to the expected, theoretical frequencies. The first comparison was made between the random generated lattice and the theoretical Poisson point process that defines complete spatial randomness (CSR). The low value of χ^2 $(p = 0.99)$ provides confidence that our lattice generating procedures were accurate. It was also apparent (Table IV) that the distributions of α_{min} for both the clustered and periodic displaced lattices were significantly different.

The distribution of α_{min} in $\mathscr{D}(S)$ of each of the three dentin specimens was averaged and compared with the simulated lattices. The best agreement was obtained for the displaced lattice with $D/D_o = 0.20$. The random (CSR) and clustered distributions were in poor agreement with the dentin values. Thus, analysis of α_{min} in $\mathscr{D}(S)$ provides evidence that there was an underlying order to the arrangement of dentin tubules, although we must emphasize that the symmetry of this underlying order was not determined in this study. A square lattice was chosen for comparison only because of its simplicity and not because of any predisposed belief that odontoblasts nucleate in a square pattern.

Boots [16] derived the pdf for the maximum angles, α_{max}, in $\mathscr{D}(S)$. The frequency distribution of α_{max} is provided in Table III for the simulated lattices and the dentin specimens. The χ^2 test between the observed random simulation and the Poisson point process (CSR) is similar in magnitude to that observed for α_{min}. From the analysis of α_{max}, it is highly unlikely $(p < 0.01)$ that the observed tubule patterns in dentin are random or

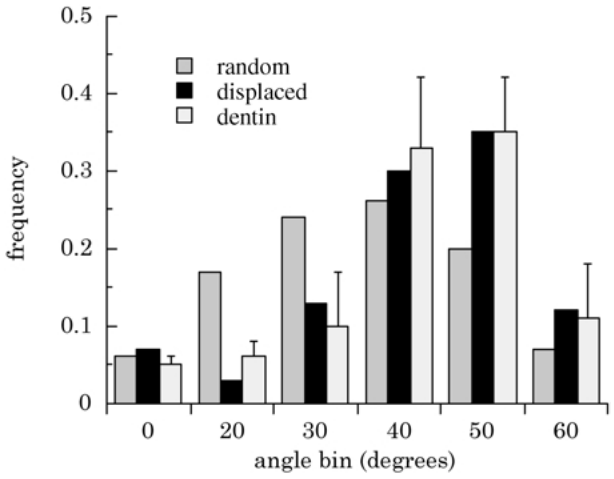

Figure 8 The frequency distribution of minimum angles of $\mathscr{D}(S)$ for the random, displaced, and dentin averages.

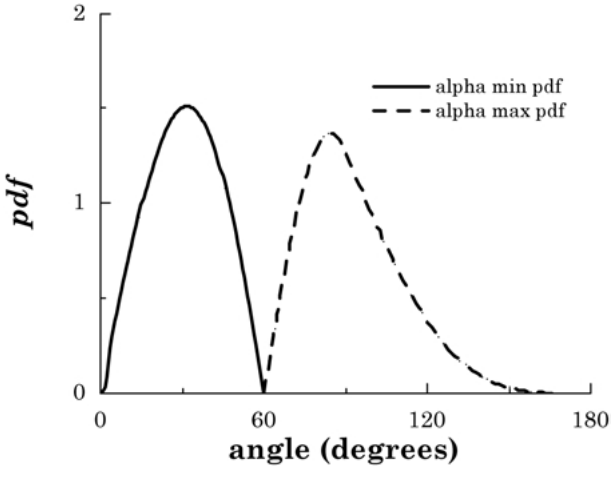

Figure 9 The theoretical probability distribution functions for α_{min} and α_{max} in $\mathscr{D}(S)$ for a random Poisson point process.

TABLE V Results of Chi-square analysis of observed patterns with expected patterns for the maximum angles in $\mathscr{D}(S)$. The one-tailed probability of obtaining a value of χ^2 or greater is given by p

Observed frequency	Expected frequency	χ^2	p
Random lattice	Random (CSR)	0.13	0.98
Clustered	Random (CSR)	40.7	$\ll 0.001$
Displaced 15%	Random (CSR)	9.2	0.01
Displaced 20%	Random (CSR)	9.5	< 0.01
Dentin average	Random (CSR)	24.9	$\ll 0.001$
Dentin average	Clustered	67.8	0
Dentin average	Displaced 0.15	3.9	0.14

clustered. In addition, the hypothesis that the tubule patterns are fluctuations about a periodic lattice cannot be rejected $(p = 0.14)$. The correlation between the observed tubule patterns and the displaced periodic lattice, however, was weaker for α_{max} than α_{min}. This was not unexpected, since the large angle tail of the distribution function (Fig. 8) was only weakly populated for any distribution. Therefore, one would expect that α_{max} would be less sensitive to differences in point pattern symmetry than α_{min}.

Angle analysis could also be performed on the interior angles of the Voronoi polygons. However, as there is a complimentarity in angle between the angles of the Delaunay triangles and the interior angles of the Voronoi polygons, it is unlikely that further analysis of the angular distributions of the vertices of the Voronoi polygons will provide any additional insight into tubule arrangement. Therefore, because it was easier to calculate the angles in $\mathscr{D}(S)$ we did not perform the angular analysis of the Voronoi diagram.

Shannon and Weaver [15] were among the first to apply the entropy statistic, H, as a measure of organization. There are problems with the use of H as a measure of organization, however. Chief among these is that the density of points affects the value of the entropy statistic, making comparisons among specimens with different tubule densities problematic. Lenz [9] proposed using the Thiel's redundancy measure, R^*, to avoid this difficulty, and successfully applied this measure to test for randomness of settlement distributions in a problem in geographical analysis.

The expectation of the redundancy measure, R^*, for an infinite, random distribution of points is 0.134, close to the value that we obtained for the simulated random distribution [18]. The value of R^* for the regular lattice was identically zero, as anticipated from inspection of Equations 4 and 5. Clustered point patterns gave values of R^* that were larger than those found for a random distribution, and for our simulated patterns were more than three-fold larger than the average for our random patterns. Thus, the redundancy measure was useful for distinguishing between the different classes of point pattern distributions.

The redundancy factor never reached the expectation of the random distribution, even for large displacements. This was most likely because the displacements were averaged about the original periodic lattice sites; hence, the vestigial order had not been removed. The random displacements appeared like noise added to the signal of underlying periodic lattice symmetry; the noise was never able to completely overwhelm the underlying signal.

A one-way ANOVA indicated that the values of R^* for the dentin specimens were significantly lower than those of the random and clustered distributions, and that there were no statistically detectable differences in R^* between the teeth. Evaluation of Fig. 5 indicates that R^* measured in the dentin specimens was consistent with a periodic array of lattice sites about which the tubule lumens were randomly displaced. The value of this displacement was not large $(D/D_o \sim 0.2)$.

In summary, geometric methods of point pattern analysis provide evidence that tubules are neither random nor clustered in human dentin. Both angular distribution analysis and redundancy measures suggest instead that tubules are highly ordered. A model of random displacements localized about periodic lattice sites describes the distribution of tubules in human dentin, although from the present data it is not yet possible to determine the underlying symmetry of this lattice. Stochastic geometric models of microstructure will be valuable in developing improved mechanical and transport models for heterogeneous materials such as dentin.

Acknowledgments

Support for this work was provided from the National Institutes of Health, NIDCR, through grant PO1 DE09859 and RO1 DE11526.

References

1. R. GARBEROGLIO and M. BRANNSTROM, *Arch. Oral Biol.* **21** (1976) 355.
2. D. H. PASHLEY, *Scan. Microsc.* **3** (1989) 161.
3. D. H. PASHLEY, A. OKABE and P. PARHAM, *Endo. Dent. Traumatol.* **1** (1985) 176.
4. J. H. KINNEY, M. BALOOCH, G. M. MARSHALL and S. J. MARSHALL, *Arch. Oral Biol.* **44** (1999) 813.
5. J. H. KINNEY, M. BALOOCH, D. L. HAUPT, S. J. MARSHALL and G. W. MARSHALL, *J. Dent. Res.* **74** (1995) 1179.
6. J. M. WHITE, H. E. GOODIS, S. J. MARSHALL and G. W. MARSHALL, *J. Dent. Res.* **73** (1994) 1560.
7. G. W. MARSHALL, M. STANINEC, Y. TORII and S. J. MARSHALL, *Scan. Micros.* **3** (1989) 1043.
8. J. H. KINNEY, M. BALOOCH, G. W. MARSHALL and S. J. MARSHALL, *Arch. Oral Biol.* **38** (1993) 1003.
9. R. LENZ, *Geographical Anal.* **11** (1979) 374.
10. G. P. CHAPMAN, *Econ. Geography* **46** (1970) 317.
11. J. G. BERRYMAN and S. C. BLAIR, *J. Appl. Phys.* **60** (1986) 1930.
12. P. B. CORSON, *J. Appl. Phys.* **45** (1974) 3171.

13. B. N. BOOTS, *Prof. Geographer* **27** (1975) 426.
14. R. E. MILES, *Math. Biosciences* **6** (1970) 85.
15. K. V. MARDIA, R. EDWARDS and M. L. PURI, *Bull. Intern. Statist. Institute* **47** (1977) 93.
16. B. N. BOOTS, *Geographical Analysis* **18** (1986) 250.
17. C. E. SHANNON and W. WEAVER, in ''The Mathematical Theory of Communication'' (University of Illinois Press, Urbana, 1949).
18. A. OKABE, B. N. BOOTS and K. SUGIHARA, in ''Spatial Tessellations: Concepts and Applications of Voronoi Diagrams'' (John Wiley and Sons, Chichester, 1992).

Received 21 April
and accepted 27 June 2000